Clays and Clay Minerals, Vol. 56, No. 2, 259–271, 2008.

INTERACTION OF AQUEOUS ACIDIC-FLUORIDE WASTE WITH NATURAL TUNISIAN SOIL

NOUREDDINE HAMDI* AND EZZEDINE SRASRA

Unité Matériaux, Technopole de Borj Cedria, Tunis, BP 95-2050 Hammam Lif, Tunisia

Abstract—Clayey soils are essential materials used to reduce hydraulic conductivity and pollutant migration, common at sites of waste disposal. This study investigates the possible use of a Tunisian soil as a lining material for disposal sites for acidic-fluoride wastes. A permeability test on a waste-solution sample (pH = 2.7) obtained from a disposal site in southern Tunisia was conducted over a period of about 2 years. The test results show that the permeability decreased with time until stabilized at 8.33×10^{-11} m/s. After the permeability test, the samples retrieved from the permeameter show a degradation state which varied with the thickness of the specimen. These samples can be classified into three zones (Z1: unaffected, Z2: moderately affected; and Z3: extensively affected). Physicochemical characterization of the three samples (Z1, Z2, and Z3), and of the original argillaceous soil, was by X-ray diffraction, Fourier transform infrared spectroscopy, differential thermal and thermal gravimetric analysis, ^{29}Si and ^{27}Al nuclear magnetic resonance, and N_2-adsorption techniques. The original sample consists essentially of palygorskite, kaolinite, and quartz. Sample Z3 underwent complete dissolution of kaolinite which supports the precipitation of fluoroaluminate and the appearance of an X-ray amorphous silica phase. In samples Z1 and Z2, the soil adsorbs fluoride at a rate of ~68.5 mg/g and is highly resistant to acidic attack.

Key Words—Acidic-fluoride Waste Storage, Clay, DTA-TG, FTIR, Permeability, ^{29}Si and ^{27}Al NMR, XRD.

INTRODUCTION

Fluoride-contaminated wastes are generated by many industrial processes including the manufacture of fertilizers and textiles. Argillaceous material is regarded as a possible host for disposal of fluoride waste (Kau *et al.*, 1997a and 1998). Therefore, it is important to understand the properties of the clays in the argillaceous material. The long-term evolution of the waste in its environment is crucial in assessing the performance and the safety of the disposal site.

Little research has been done on the interaction of acidic-aqueous fluoride waste with clay minerals (Kau *et al.*, 1997a; Peterson and Gee, 1985). The permissible limit of fluoride in drinking water is 1.5 mg/L according to the World Health Organization guidelines (WHO, 1993). Therefore, the sorption rate and the transport behavior of the pollutant in the clay liner material are crucial in terms of protecting ground water and in the assessment of the long-term mobility of the fluoride contaminant.

Adsorption of fluoride in aluminosilicates is essentially related to the presence of alumina in the structure, as its point of zero charge (pzc) reaches a value of up to 8.3. The other main constituent, silica, possesses a pzc of 2.5 in the experimental pH range, resulting in little adsorption of fluoride (Chaturvedi *et al.*, 1988). The adsorption concept for kaolinite, presented by Kau *et al.* (1997b), may be viewed in terms of equation 1, where the sorption process is defined as an equilibrium reaction.

$$(\text{clay} - \text{OH})_{(s)} + F^- \rightleftharpoons (\text{clay} - \text{F})_{(s)} + OH^-_{(aq)} \qquad (1)$$

Additionally, for low pH (<3), Kau *et al.* (1997a) showed that the removal of fluoride by clay is achieved by means of sorption. It also involves the precipitation of some fluoroaluminates such as chiolite ($Na_5Al_3F_{14}$ or $5NaF{\cdot}3AlF_3$). We were unable to find any published work on the subject of the dissolution mechanism of palygorskite in HF solution. Most such work focuses on acidic activation of palygorskite by HCl in order to increase the specific surface and adsorption properties (*e.g.* Cai and Xue, 2004; Myriam *et al.*, 1998; Gonzalez *et al.*, 1989).

The objective of this research, therefore, was to investigate the interaction of natural argillaceous soil with acidic-fluoride wastes, in order to elucidate the reaction between them, particularly in the case of a clayey Tunisian soil. This study considered the long-term permeability of the clay in order to follow the evolution of the reaction between it and the acidic-waste solution and its effects on the soil. This study also aimed to identify the precipitated fluoride products, and to establish the mechanism of clay dissolution, using analytical techniques including X-ray diffraction (XRD), Fourier transform infrared spectroscopy (FTIR), differential thermal and thermal gravimetric analysis (DTA-TG), ^{29}Si and ^{27}Al nuclear magnetic resonance (NMR), and textural study by means of N_2-adsorption.

* E-mail address of corresponding author:
hamdinoureddine@yahoo.fr
DOI: 10.1346/CCMN.2008.0560209

Table 1. Mineralogical composition of the starting sample.

Composition of starting sample	%
Palygorskite	59.5
Kaolinite	12.9
Quartz	23
Calcite	3.2
Dolomite	0.8
Feldspar	0.6
CEC (meq/100 g) = 22.6	
S_{BET} (m^2/g) = 66.8	
pH = 8.6	

Table 2. Composition of the leaching solution.

Ions	Initial concentration in waste water (mg/L)
F^-	2360
Cl^-	880
PO_4^{3-}	1500
Na^+	2836
Ca^{2+}	850

EXPERIMENTAL

Materials

The argillaceous soil used in this study was collected from the southeast of Tunisia; when placed in distilled water, it gives a basic pH of 8.6 (Table 1). The soil sample was taken from a depth of 16.1 m at a site reserved for the storage of industrial waste. It was used in its natural state in the permeability test and for all other analyses. The quantitative mineralogical analysis was extracted from the powder XRD data using an internal standard for each mineral (Jozja, 2003; Cody and Thompson, 1976). The clay fraction was quantified, after purification, using the same method as above, and based on a pure, standard clay mineral. The mineralogical composition of this sample, the cation exchange capacities (CEC), and the specific surface areas (S_{BET}) are summarized in Table 1. The industrial waste to be disposed of consists of significant amounts of solid combined with a liquid solution of pH 2.7; the waste contains large amounts of harmful material, including fluoride with a concentration of 2360 mg/L. Phosphates and chlorides are also present, but at lesser concentrations (Table 2).

Permeability determination

Permeability tests were carried out as per the procedure described in ASTM D5084 (ASTM, 1991) using a 'Tecnotest' permeameter; as described by Hamdi *et al.* (2005), the soil specimen was placed between two porous discs (Figure 1). The initial head, h_1, was recorded at time $t = 0$, and then the liquid was allowed to flow through the soil in order to obtain h_2, the final head, at time t. The hydraulic conductivity, k, was calculated by the following equation:

$$k = 2.303\frac{aL}{At}\log\frac{h_1}{h_2} \quad (2)$$

where k is the hydraulic conductivity (cm s^{-1}), A is the cross-sectional area of the specimen (cm^2), a is the cross-sectional area of the standpipe (cm^2), and L is the length of specimen (cm).

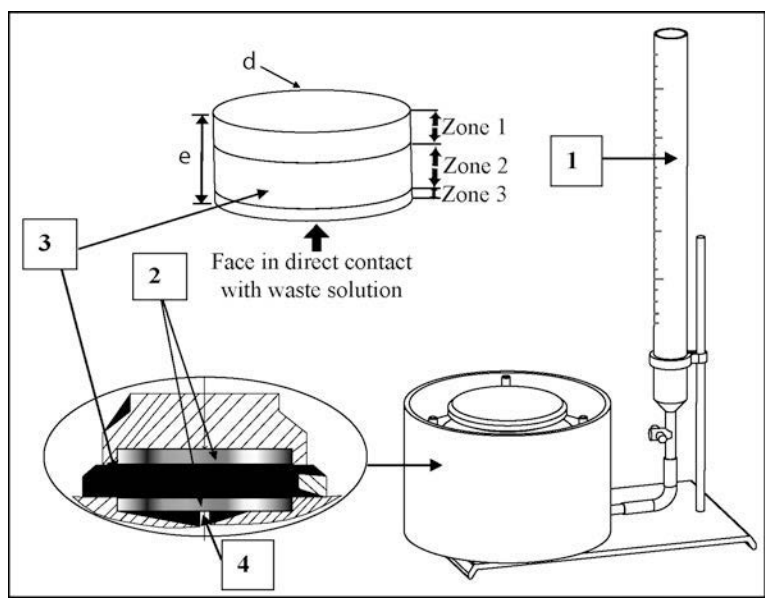

Figure 1. Permeameter: (1) graduated burette, liquid cell outer diameter = 8 mm; (2) porous discs; (3) sample (soil), e = 2 cm, d = 71.4 cm; (4) entry point of liquid.

https://doi.org/10.1346/CCMN.2008.0560209 Published online by Cambridge University Press

XRD

Powder XRD patterns were obtained using a PANalytical X'Pert HighScore Plus diffractometer in the range 3−60º2θ, at a scanning rate of 2º min^{-1} and employing CuKα filtered radiation.

IR spectroscopy

The IR spectra were recorded using a Perkin Elmer 783 spectrophotometer. The samples were used in pellet form containing 2 mg of clay mixed and pressed with 200 mg of KBr.

Chemical analysis

The clay samples were attacked by a mixture of three acids (HCl, H_2SO_4, HNO_3). All elements were dissolved into solution except for the Si which was determined by gravimetry. The Al, Fe, Mg, Ca, Na, and K were assayed by atomic absorption spectrophotometry (AAS Vario 6), fluoride was analyzed by means of a F-selective electrode (Metrohm 781 pH/ion meter), and the phosphate concentrations were measured by the 'ASTM Standard Method', (APHA, AWWA, WPCF, 1995, *i.e.* vanadomolybdophosphoric acid colorimetric method) using the spectrophotometer Hach DR/4000.

The analytical errors are 5% for Al, Fe, Mg, Ca, Na, and K, and 10% for Si, F, and P.

Thermal analysis

Differential thermal analysis (DTA) and thermal gravimetric (TG) analysis were performed using a SETSYS Evolution-1750 instrument. Approximately 10−20 mg samples were placed in a platinum crucible on the pan of a microbalance, and then heated from room temperature to 800ºC at a heating rate of 10ºC/min while being purged with argon at a flow rate of 100 mL/min and being weighed constantly.

NMR spectroscopy

The NMR characterizations of the starting and treated samples were carried out on an MSL 360 Bruker solid-state, high-resolution NMR spectrometer, equipped with 7.05T wide-bore superconducting magnets at 59.62 and 78.20 MHz for ^{29}Si and $^{27}A1$ NMR spectra, respectively. The ^{29}Si spectra were acquired using 8 kHz spinning frequency with a 90º pulse of 5 μs and a recycle time of 6 s, and were referenced to tetramethylsilane (TMS). The ^{27}Al spectra were acquired using an 8 kHz spinning frequency with a 15º pulse of 6 μs and recycle time of 1 s and were referenced to $AlCl_3 \cdot 6H_2O$.

CEC and texture analysis

The CEC was determined using the copper ethylendiamine ($(EDA)_2CuCl_2$) complex (Bergaya and Vayer, 1997): the CEC was calculated from the quantity of $Cu(EDA)_2^{2+}$ adsorbed by the clay (*i.e.* the amount initially added to the clay suspension minus the amount remaining in the supernatant solution after adsorption and centrifugation). The specific surface area was measured at 77 K by the BET method with a Quantachrome Autosorb-1 instrument using N_2 gas. The total pore volume was derived from the amount of nitrogen adsorbed at a relative pressure close to unity (p/p_o = 0.99) by assuming that all accessible pores had been filled with condensed nitrogen in the normal liquid state.

RESULTS AND DISCUSSION

Permeability

At the point of water saturation, the permeability of this soil is in the order of 2.5×10^{-10} m/s. The results of the permeability of the waste water are given in Figure 2. The curve shows the variation of permeability as a function of time. The permeability using wastewater

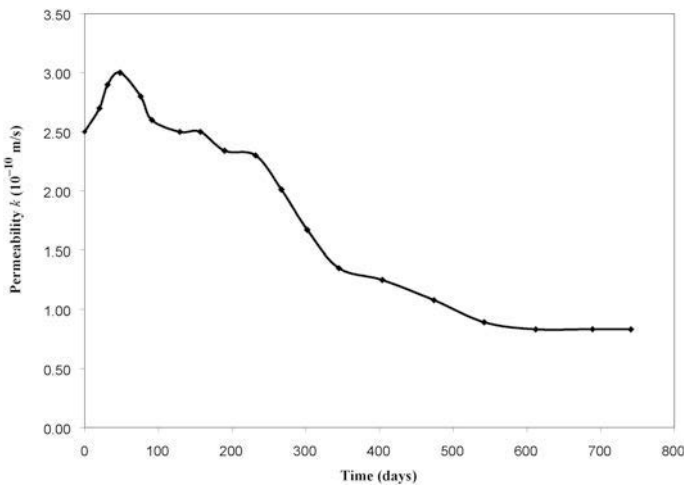

Figure 2. Variations in the permeability of sample by acidic-waste solution with time.

https://doi.org/10.1346/CCMN.2008.0560209 Published online by Cambridge University Press

Table 3. Composition (wt.% oxide) of the starting soil and of samples from each of the three zones which have recuperated after the permeability test.

	SiO_2	Al_2O_3	Fe_2O_3	MgO	Na_2O	CaO	K_2O	F	P_2O_5	I. Lo
Starting soil	64.5	8.77	4.78	2.78	0.73	3.61	1.74	0.02	0.07	13.2
Z1	73.8	6.93	3.19	1.90	1.42	1.89	1.40	0.42	0.18	8.3
Z2	68.6	6.59	2.87	1.60	1.89	3.52	1.60	1.87	0.74	10.9
Z3	62.4	6.33	2.55	0.89	6.12	5.22	1.72	2.63	1.28	11.7

decreases with time from 2.5×10^{-10} to 8.33×10^{-11} m/s within 741 days. This decrease in permeability could be explained by structural variations, *i.e.* reductions in the pore size, and by the halt of water flow by precipitates formed from pollutants in the soil, which indicates the integrity of the clay and its superior resistance to acid attack.

Following the permeability test using the waste-water solution, the specimen was removed from the permeameter. The sample retrieved shows a variation in terms of the degree of degradation and formation of precipitates, varying with different levels in the soil specimen. The sample was divided into three parts depending on the state of acid attack (Figure 1). The first part, Zone 1 (Z1), was the top of the specimen which had a chestnut color, comparable with the initial clay; the second part, Zone 2 (Z2), was from the middle of the specimen, and had a clear and somewhat lighter chestnut color; the third part, Zone 3 (Z3), from the bottom of the specimen, <2 mm thick, was in direct contact with the acid solution, and was almost white in color.

Chemical analysis

Table 3 shows the chemical composition (wt.%) data of the clayey soil before and after the permeability test. The data indicate that the percentage of SiO_2 in all the samples was relatively high. This is consistent with the presence of quartz as shown by XRD (Figure 3). After the permeability test, the concentrations of Al, Mg, and Fe ions decreased in all zones; this was caused by the acidic dissolution of kaolinite and palygorskite, confirmed by the XRD analysis. For Z1, most of the Ca was removed because of the acid dissolution of calcite (%CaO decreased from 3.61 to 1.89%). On the contrary,

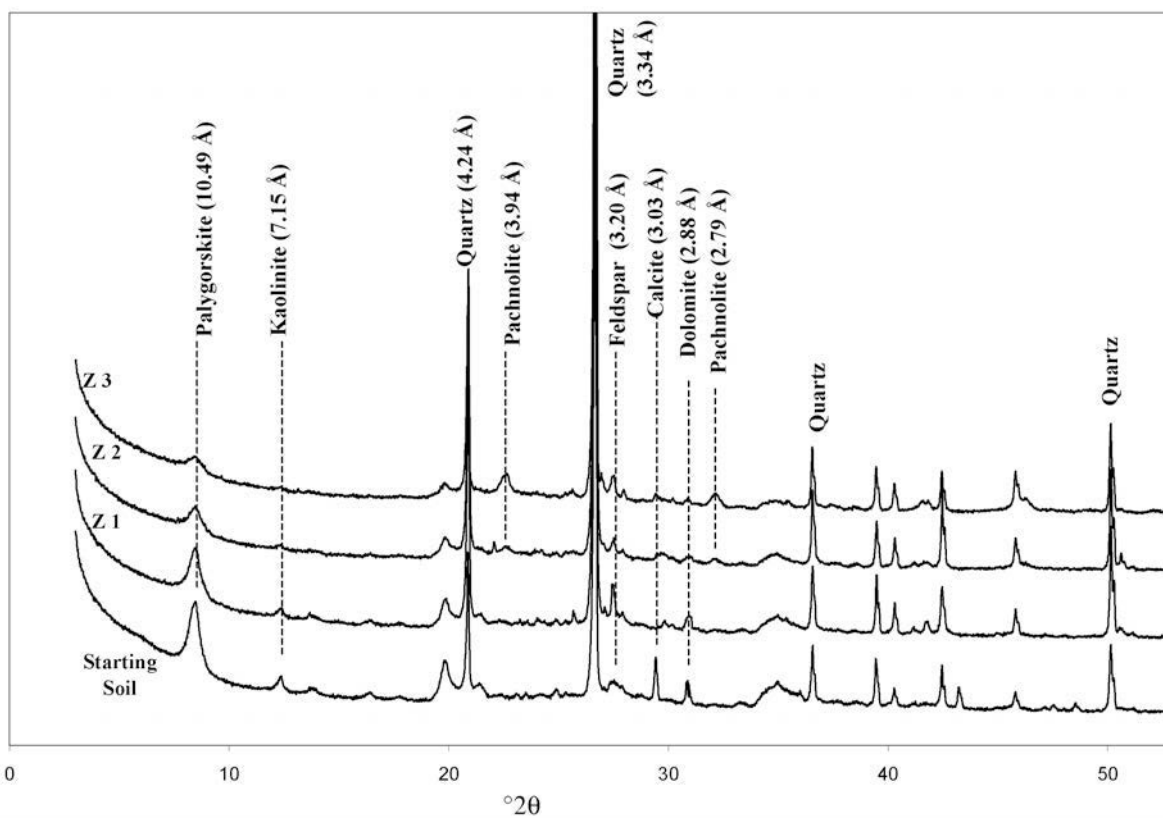

Figure 3. XRD patterns of starting clay and of samples from the three zones (Z1–Z3) which have recuperated after the permeability test.

https://doi.org/10.1346/CCMN.2008.0560209 Published online by Cambridge University Press

for Z2 and Z3, the percentage of CaO increased, due to the adsorption of Ca (which was present in the leachate) onto the clay. Similar results were obtained in the case of Na. On the other hand, there was a notable increase in the concentration of fluoride and phosphate from sample Z1 to Z3, after the permeability test. The largest amount of F (2.63%), in Z3, is in good agreement with the formation of pachnolite in the same zone, as observed by XRD.

Mineralogical composition

Figure 3 presents the XRD patterns of raw and leached samples. As shown, this soil essentially comprises palygorskite and a small amount of kaolinite. The associated minerals are quartz, calcite, dolomite, and feldspar. X-ray diffraction analysis of the treated samples showed a decrease in peak intensity for kaolinite (reflection at 7.15 Å) which reached almost zero for Z3 (Figure 3), reflecting the dissolution of kaolinite. Though the intensity of the palygorskite peaks (reflection at 10.49 Å) also decreased, peaks persist in analyses of Z3. This indicates that palygorskite is more resistant to acidic attack than kaolinite. An explanation for this is that the Al−O bonds are considerably more prone than Si−O bonds to attack by acidic-fluoride solution (Kau *et al.*, 1997a), as determined by the level of each bond type in the aluminosilicate 2:1 clay type, such as palygorskite. The peaks for calcite and dolomite (reflections at 3.03 Å and 2.88 Å, respectively) disappeared even for Z1. The XRD patterns of Z2 and Z3 (Figure 3) show the presence of new peaks appearing at 3.94 and 2.79 Å, corresponding to *hkl* reflections of 220 and 224 for pachnolite ($CaNaAlF_6(H_2O)$). However, under acidic conditions, the Al ion derived from clay dissolution reacted with the free fluoride, Na, and Ca obtained from waste-water solution after calcite dissolution. This allows the product to be described by equation 3.

$$Ca^{2+} + Na^{+} + 6F^{-} + Al^{3+} \rightleftharpoons CaF_2 + NaF + AlF_3 \quad (3)$$

FTIR spectroscopy

Figure 4 shows the FTIR spectrum of a natural soil sample containing quartz (798 cm^{-1}) and calcite (1430 cm^{-1}). The calcite disappeared from all zones after the permeability test. An asymmetric band, centered at 1645 cm^{-1}, appeared in all zones. This corresponds to the bending modes of adsorbed and zeolitic water (Suárez and García-Romero, 2006). The structural OH-stretching band at 3615 cm^{-1}, together with the well defined AlAlOH deformation band at 912 cm^{-1}, and a slight inflection near 860 cm^{-1} (AlMgOH), reflect the mainly dioctahedral character of palygorskite (Madejová and Komadel, 2001). The intensity of the absorption bands at 3615, 912, and 860 cm^{-1} decreased and almost disappeared for sample Z3. In addition, Si-O-Si deformation bands appeared at 479 cm^{-1}, and the characteristic bands of Si−O stretching modes were indicated by bands at 986, 1030, and 1194 cm^{-1}(Madejová and Komadel, 2001). In the case of Z3, the Si−O stretching bands at 1090 cm^{-1} became dominant. This is due to the formation of an X-ray amorphous silica phase (Temuujin *et al.*, 2004).

NMR spectroscopy

^{29}Si NMR spectra. Figure 5 shows the ^{29}Si NMR spectra of the starting sample with two well resolved resonances

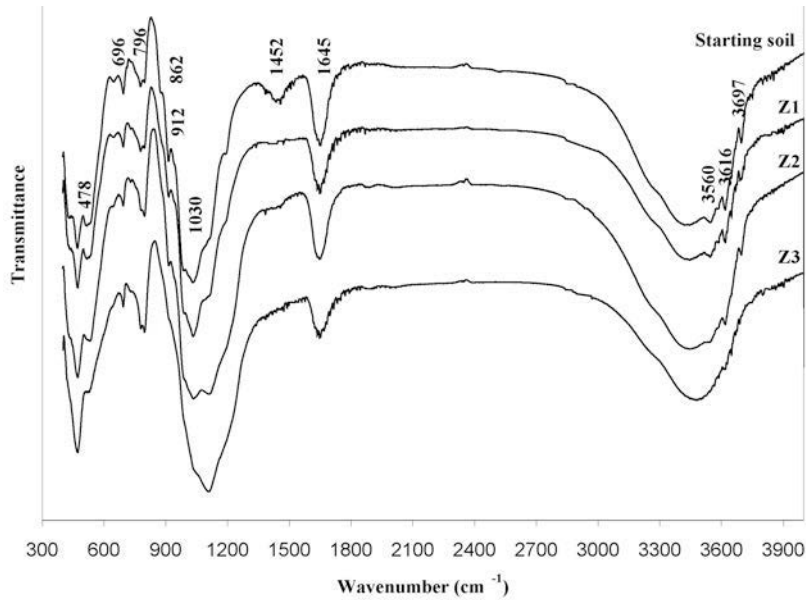

Figure 4. IR spectra of starting clay and of samples from the three zones (Z1−Z3) which have recuperated after the permeability test.

https://doi.org/10.1346/CCMN.2008.0560209 Published online by Cambridge University Press

at −91.6 and −107 ppm. In addition, two less intense resonances at −97.2 and −85 ppm were also observed. However, the spectra at −91.6 and −97.2 ppm, have previously been attributed to two specific Q^3 (O−Al) sites of palygorskite (Komarneni *et al.*, 1986; Barron and Frost, 1985). The minor resonance at 85 ppm is attributed to Q^2 (Si−OH) Si nuclei (Kuang *et al.*, 2004). As established earlier, the resonance at −107 is characteristic of quartz (Spearing and Stebbins, 1989; Fiske *et al.*, 1998). For Z1 NMR spectra, no great variations from spectra of the starting mineral were observed. In the case of Z2, the NMR spectra show two resolved resonances at −100 and at −111 ppm formed under acid treatment and assigned to Q^3(1OH) and Q^4 in an X-ray amorphous hydrous silica phase (Engelhardt and Michel, 1987). In Z3, where the clay is in direct contact with acidic waste, the dissolution is very important, reflected through the decreased resonance intensity of peaks relative to Q^3(0Al), Q^3(1OH), and quartz. However, the peak intensity of Q^4 increases. For sample Z3, the peak intensity for Q^3 (O−Al) disappeared, indicating the maximum destruction of clay structure.

^{27}Al NMR spectra. The ^{27}Al NMR spectra of the initial sample and of the treated waste samples are reported in Figure 6 and provide very interesting information on the changes in the local structure of the clay samples. The results for the initial sample are indicated through a sharp peak at 4.2 ppm corresponding to octahedral Al in palygorskite (Kinsey *et al.*, 1985). After acid treatment of the Z1, Z2, and Z3 samples, a small peak appeared at ~60 ppm, related to a trace of tetrahedral Al which became visible after degradation of carbonate and some of the octahedral sheet. The assignment of Al to tetrahedral or octahedral coordination is based on previous studies (Muller *et al.*, 1981; Fyfe *et al.*, 1983; Komarneni *et al.*, 1986). In the case of Z2 and Z3, the shift of the initial peak from 4.2 to 3.6 and 2.6, respectively, was attributed to the acid attack (Kiyoshi *et al.*, 2006; Imre *et al.*, 1999). Figure 6 (sample Z3) shows a resonance peak at −4.7 (Jerry and Hellmut, 2001; Dirken *et al.*, 1992) which corresponds to the octahedral coordination of Al by F (fluoride) in pachnolite fluoroaluminate ($CaNaAlF_6$). Thus, the peaks at the sides of the Al spectra are due to spinning sidebands (SSB).

Thermal analysis

The thermal properties of palygorskitic clay have been studied by many (*e.g.* Guggenheim and Koster Van Groos, 2001; Viseras and Lopez-Galindo, 1999; Kuang *et al.*, 2004; Gonzalez *et al.*, 1989). The DTA and TG analyses of the present crude sample (Figure 7a) are in general agreement with data from previous investiga-

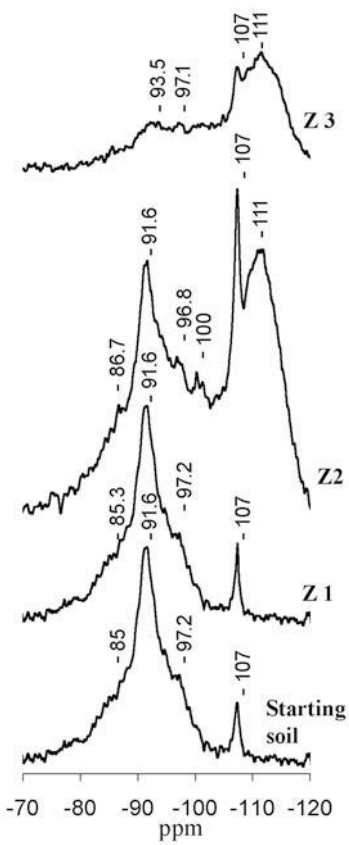

Figure 5. ^{29}Si NMR spectra of samples before and after the permeability test.

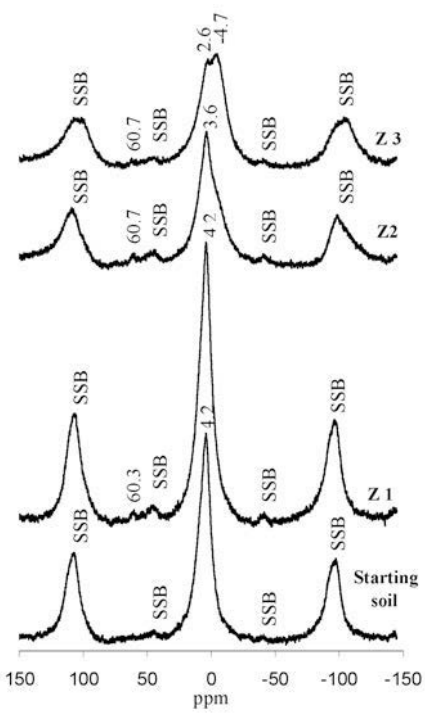

Figure 6. ^{27}Al NMR spectra of samples before and after the permeability test.

https://doi.org/10.1346/CCMN.2008.0560209 Published online by Cambridge University Press

tions. The first large endothermic reaction, at ~120ºC, corresponding to ~10 wt.% loss between 27 and 170ºC, is attributed to the release of water adsorbed on the external surface and in the channels (zeolitic water) of palygorskite; the amount depended on relative humidity or water-vapor pressure. The second endothermic reaction took place at ~240ºC with a weight loss of 2.5% (at 170−300ºC), and can be attributed to the release of crystalline H_2O, presumably bound at layer edges in the palygorskite channels (Guggenheim and Van Groos, 2001; Kuang *et al.*, 2004) (Figure 13). The third endothermic reaction at 500ºC with a weight loss of 7.9 wt.% (at 300−600ºC) is attributed to the sum of weight lost due to structural dehydroxylation of the palygorskite (Kuang *et al.*, 2004) and the kaolinite (Carolina *et al.*, 2002). After the permeability test, the dissolution of kaolinite and palygorskite was, therefore, represented by the decrease in the intensity of the third endothermic peak at 500ºC for Z1, which disappeared completely in samples Z2 and Z3 (Figure 7). For all samples, a sharp endothermic peak appeared immediately after the third endothermic peak at ~576ºC, which was assigned to the allotropic transformation of α-quartz to β-quartz (Mackenzie, 1970; Monteiro *et al.*, 2005). In addition, comparing the DTA patterns of Z3 to the starting sample (Figure 7) revealed a downward shift of the first and second endothermic peaks from 120 to 102ºC and from 240 to 218ºC, respectively. The corresponding TG patterns also revealed a decrease in the rate of weight loss, reaching 2.7 and 0.9 wt.%, respectively, compared to 9.8 and 2.9 wt.% for the initial sample. At high temperature (>600ºC), a small weight loss was observed, which is associated with the X-ray amorphous product phase after acid attack.

Texture analysis and CECs

The shape of the N_2 adsorption-desorption isotherms (Figure 8) of the unleached and leached clay samples (Z1, Z2, and Z3) was similar to type II in the IUPAC classification system and typical of macroporous or nonporous adsorbents. The hysterisis was of H3 type, characteristic of layered materials with slit-shaped pores (Sing *et al.*, 1985). The decrease in adsorbed volumes of the leached samples with leaching zone can be explained in terms of decreasing numbers of pores from top to bottom of the specimens. This is due to the adsorption of ions (existing in waste solution) at the surface and the dissolution of some of the clay fraction under the acidic conditions.

The specific surface area, total pore volume, and CEC of the samples before and after the permeability test are presented in Table 4. The specific surface area decreases significantly as a function of degradation state of the specimen, from 66.8 m^2/g (starting sample) to 26.7 m^2/g (Z3 sample), due to the exchange of ions in the interlayer space and to adsorption on the surface of clay. The same results were obtained for the CEC, where the minimum (1.2 meq/100 g) was observed in sample Z3. The pore volume (Vp), however, decreased only slightly from 0.251 to 0.209 cm^3/g.

Fluoride-sorption isotherms

This fluoride sorption study was an attempt to evaluate the fluoride removal potential of the Tunisian soil. These investigations focused mainly on the determination of adsorption capacity, determined from adsorption kinetics and the effect of pH on adsorption. The rate of fluoride adsorption was found to be relatively slow and saturation persisted for more than 24 h. In addition, the percentage of adsorption increased almost linearly with the decrease in pH, although experiments with solution pH values of <4 were avoided because of reported clay dissolution under such conditions (Budd, 1961). The fluoride sorption isotherms at pH 4 were determined by using 1 g of sample and 10 mL of NaF solution at various concentrations (50−10,000 mg/L) where the pH was adjusted to 4 (where F^- is the major species in solution, see Figure 10) and the solute was diluted to 30 mL with deionized water. In the case of adsorption using waste water, the sample adsorbent (1 g) was suspended in 30 mL of waste-water solution with different concentrations, prepared by diluting the initial solution to achieve a range of concentrations from 20 to 2500 mg/L, preserving pH at 4 by adding aliquots of 0.5 M solutions of either NaOH or HNO_3. The XRD analyses of the starting and final clay during adsorption experiments (at pH = 4) showed the degradation of calcite, but neither the dissolution of the clay fraction nor fluoride precipitation was detected. This confirms that under these conditions the main phenomenon is adsorption and not precipitation. The amount of F^- sorbed (mg of F^-/g of sample) was plotted *vs.* the equilibrium F^- concentration (mg/L). The experimental sorption data for the removal of fluoride ions at pH = 4 was then compared to a plot that would be obtained assuming either the Langmuir (equation 4) or Freundlich (equation 5) adsorption isotherm model.

$$q_e = \frac{Q_m b C_e}{1 + b C_e} \quad (4)$$

Table 4. CEC, surface area (S_{BET}), and pore volume (V_P) of samples before and after the permeability test.

Sample	S_{BET} (m^2/g)	V_P (cm^3/g)	CEC (meq/100 g)
Starting soil	66.8	0.251	22.6
Z1	42.5	0.236	14.6
Z2	37.0	0.211	12.0
Z3	26.7	0.209	1.2

https://doi.org/10.1346/CCMN.2008.0560209 Published online by Cambridge University Press

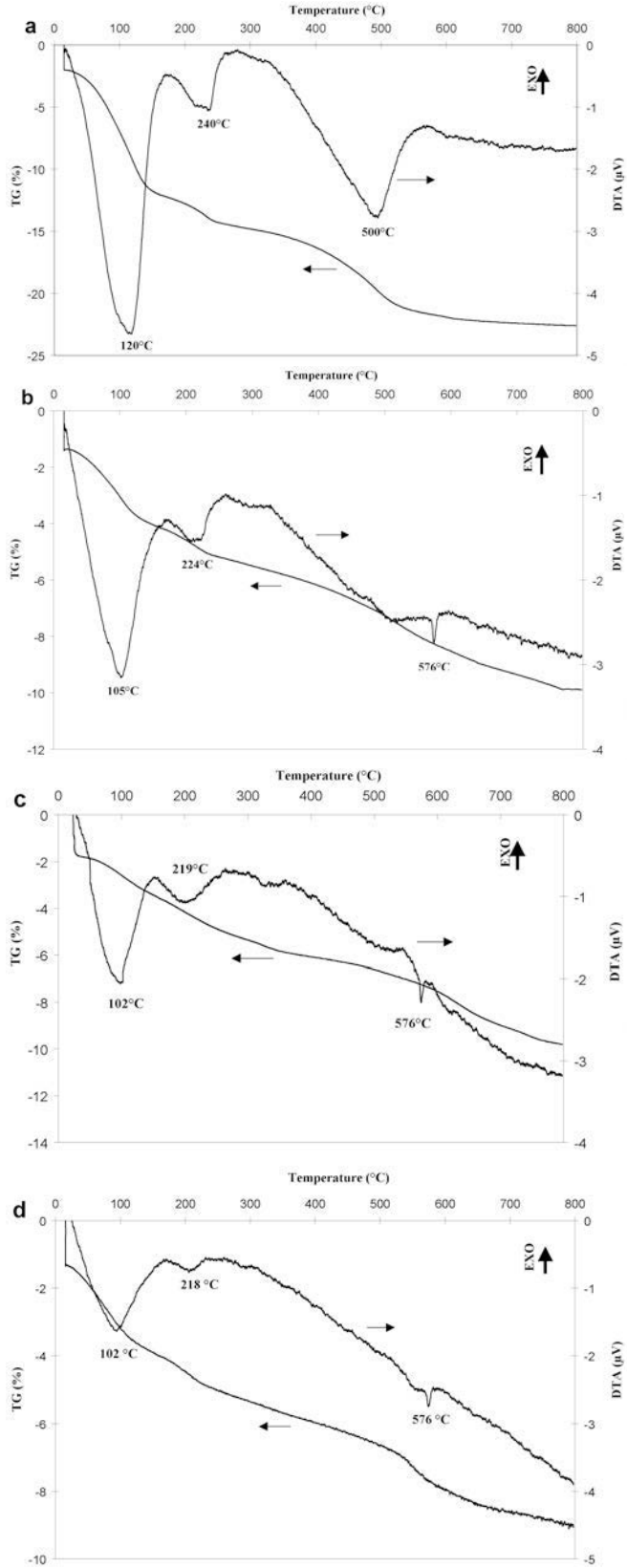

Figure 7. DTA-TG curves of: (a) starting soil; (b) sample from Z1; (c) sample from Z2; and (d) sample from Z3.

https://doi.org/10.1346/CCMN.2008.0560209 Published online by Cambridge University Press

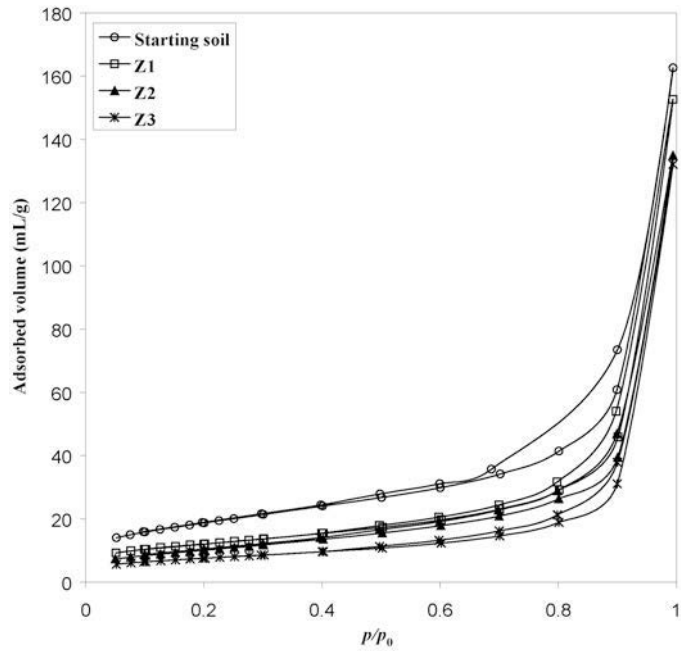

Figure 8. N_2-adsorption isotherms of the starting material and products leached after the permeability test.

$$q_e = K_F C_e^{1/n} \quad (5)$$

where q_e is the amount of adsorbate adsorbed per unit weight of adsorbent (mg/g); C_e, the equilibrium concentration (mg/L); Q_m and b, the Langmuir constants related to monolayer capacity and energy of adsorption, respectively; and K_F and 1/n, the Freundlich constants.

Figure 9 presents the experimental sorption isotherms with NaF and waste solution and the correlation using both models at pH = 4. Note that the sorptivity gradients for this soil by waste water or NaF solutions were very similar, as predicted by the modeled bonding constants. Isotherms of fluoride sorption fit the Langmuir model well, with a correlation coefficient of 0.98–0.99. The maximum sorption capacity, calculated from this model and reported in Table 5, is 68.5 mg/g for waste solution and 64.9 mg/g for NaF solution, which values are greater than for other clay minerals reported in the literature (Kau *et al.*, 1998; Chaturvedi *et al.*, 1988).

Reaction mechanism of clay minerals under acidic-fluoride solution

Two possible mechanisms of clay dissolution under acidic-fluoride solution are suggested, as shown in Figure 11, and the mechanism of attack of Si–O and Al–O bonds are assumed to be similar (Kau *et al.*, 1997a). Many previous workers (*e.g.* Bergaya *et al.* 2006; Gonzalez *et al.*, 1989; Kau *et al.*, 1997a) suggested that attack of the alumina sheet would be more favored than the silica sheet because silica is more stable in an acidic medium. This is explained by the low point of zero charge for silica (*i.e.* pH $\approx$ 2), whereas for alumina it is ~8.3. Thus, alumina is more highly charged (positively) than silica, creating greater bonding instabilities in the acidic pH region. This explains the greater dissolution rate of kaolinite than of palygorskite (Figure 3).

Palygorskite is the major fraction in this soil and its dissolution mechanism under acidic-fluoride solution apparently has not been examined before. The structural

Table 5. Estimated isotherm parameters for fluoride adsorption.

	Isotherm type					
	Langmuir			Freundlich		
Source of F^- ions	Q_m (mg/g)	b (L/mg)	r^2	K_F	1/n	r^2
Waste solution	68.5	$6.65\ 10^{-3}$	0.988	0.67	0.75	0.982
NaF solution	64.9	$4.48\ 10^{-3}$	0.991	0.33	0.87	0.990

https://doi.org/10.1346/CCMN.2008.0560209 Published online by Cambridge University Press

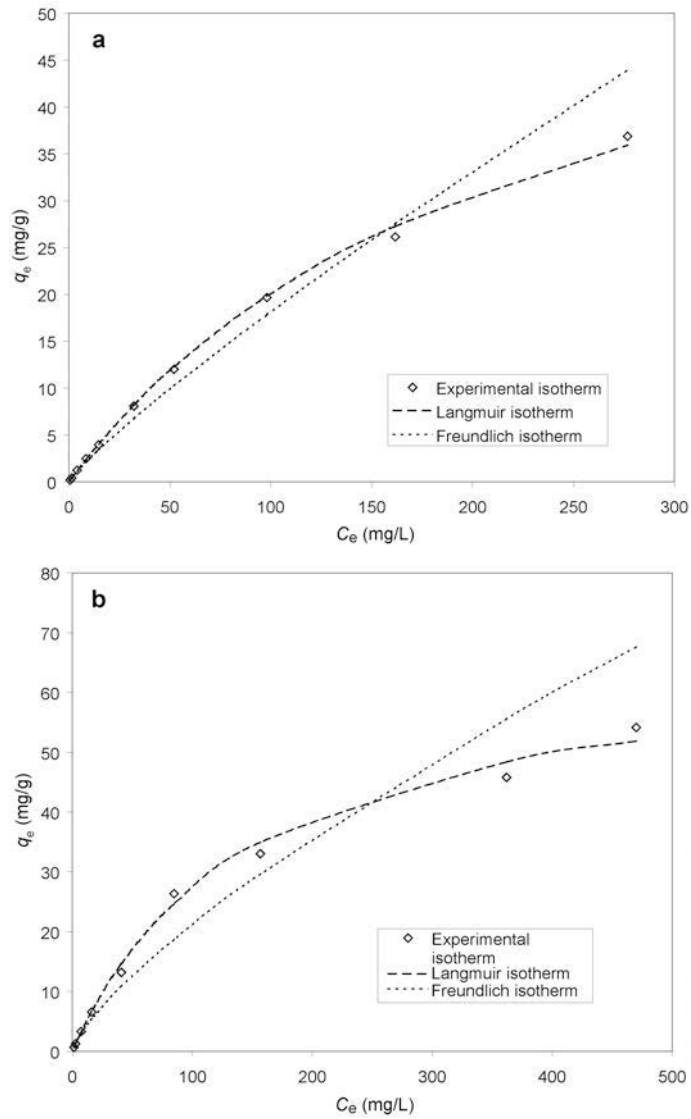

Figure 9. Fluoride adsorption isotherm at 25±2ºC and pH 4±0.2: (a) using NaF solution; and (b) using a waste solution.

evolution of palygorskite under acidic-fluoride leaching for each zone is presented in Figure 12. In these proposed mechanisms, we have taken into account the results of XRD, chemical analysis, NMR spectra, and the distribution of the fluoride species with pH (Figure 10). In the case of Z3, where the sample was in direct contact with waste solution (pH<3, where HF was the major species in the solution; Figure 10), the greatest degree of dissolution of palygorskite was observed, along with the precipitation of fluoroaluminate and formation of an X-ray amorphous silica phase. This also allowed an increase in the pH of solution due to the exchange of OH by F (equation 1). For this reason, in zones 1 and 2, the dominant reaction, apparently, is fluoride sorption with little dissolution. Hence, the chemical analysis data of Z3 have shown that dissolution of the octahedral sheet occurs in preference to that of tetrahedral sheets, because the percentages of Al_2O_3, Fe_2O_3, and MgO decreased significantly compared to that of SiO_2. This study also suggests that the dissolution reaction is caused primarily by HF and not by the individual hydrogen or fluoride ions alone.

In order to understand more fully the modification of the palygorskite structure under acidic-fluoride solution, consider two possible reaction mechanisms (Figure 13). The first shows adsorption (where pH> 4), the second reveals dissolution (where pH <2). This is according to the predominance of the fluoride species with the pH (Figure 10). Between pH 2 and 4, both phenomena (adsorption and dissolution) exist simultaneously.

https://doi.org/10.1346/CCMN.2008.0560209 Published online by Cambridge University Press

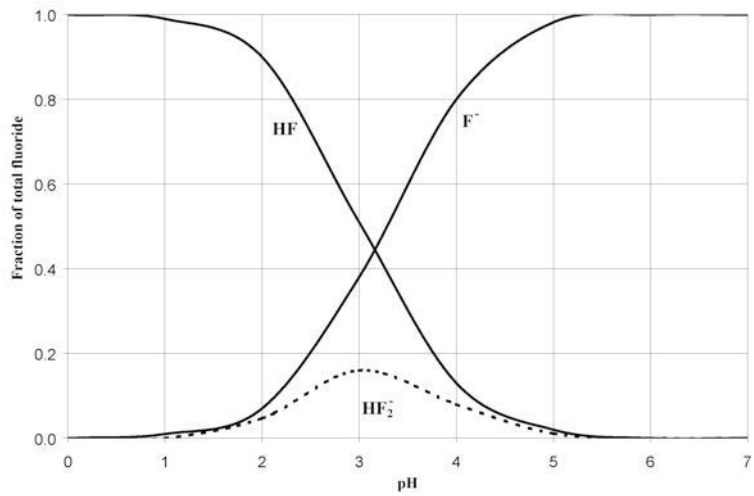

Figure 10. The species distribution diagram of 0.1 M fluoride with varying pH (Vanderborgh, 1968; Kau *et al.*, 1997a).

Furthermore, under lower pH, dissolution and precipitation are the major phenomena and the acidity of the HF solution is believed to assist in the protonation of the silica surface and thus weaken the siloxane bonds, allowing fluorinated species to react with Si, as shown in Figure 13. Hydrofluoric acid is highly toxic and corrosive and capable of chemically attacking clay-lined impoundments.

CONCLUSION

This permeability study of a Tunisian soil by aqueous, acidic-fluoride waste over a long period of time, shows that the permeability decreases as a function of time, from 2.5×10^{-10} to 8.33×10^{-11} m/s, after 741 days. However, the samples 'recuperated' after the study, indicating a degree of variation of degradation, depending on the thickness of the sample.

The XRD results revealed the structural dissolution of kaolinite and palygorskite, showing that kaolinite is more vulnerable than palygorskite. In the case of sample Z3, we observed new peaks appearing at 3.94 and 2.79 Å, attributed to precipitation of pachnolite ($CaNaAlF_6 \cdot (H_2O)$).

Comparing the materials from the three zones to the starting sample, the textural investigations suggest that Z3 presents few textural properties (S_{BET} = 26.7 m^2/g and V_p = 0.209 cc/g) which renders it non-exchangeable, with a weak CEC (1.2 meq/100 g). The results of the NMR spectroscopy confirmed the attack of the clay fraction in Z3, proven by the increase in the amount of X-ray amorphous silica phase at −111 ppm (^{29}Si NMR) and the resonance at −4.7 ppm (^{27}Al NMR) which is attributed to octahedral coordination of Al by F in pachnolite. This study also suggested that the dissolution reaction is caused primarily by HF and not by the individual hydrogen or fluoride ions alone. The results of the adsorption isotherms show that this soil has a capacity for fluoride adsorption of ~68.5 mg/g. This study eliminates a gap in our understanding of the reaction between acidic-fluoride solution and a clay mineral (palygorskite), and helps to envisage the safe

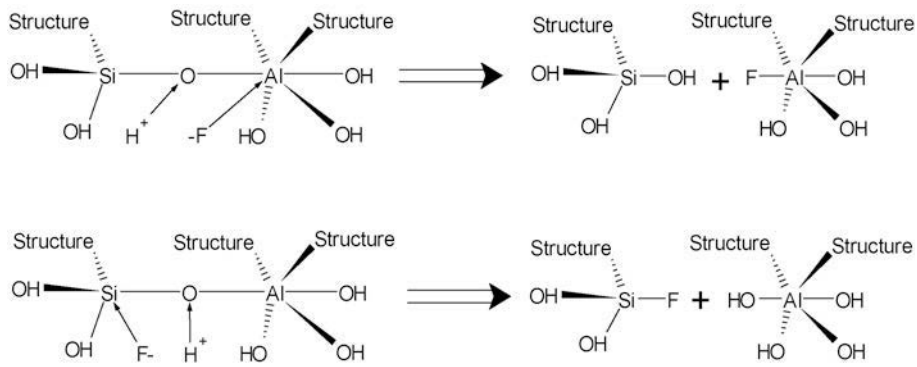

Figure 11. Dissolution of silicon-oxygen and aluminum-oxygen bonding under acidic fluoride solution.

https://doi.org/10.1346/CCMN.2008.0560209 Published online by Cambridge University Press

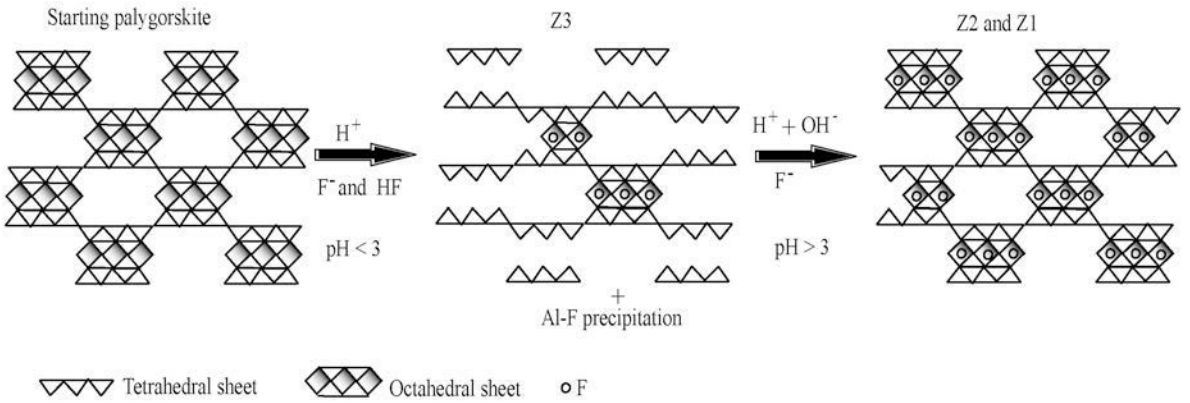

Figure 12. Schema of structural evolution of palygorskite under acidic fluoride solution.

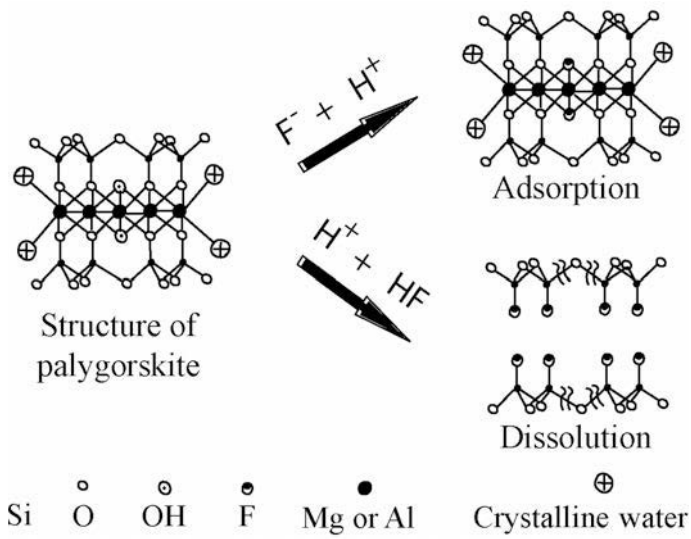

Figure 13. Schema of elementary structural evolution of palygorskite under acidic fluoride solution.

storage of HF-contaminated wastes in clay-lined landfills sites.

REFERENCES

APHA, AWWA, WPCF (1995) *Standard Methods for the Examination of Water and Wastewater*, 19th edition. APHA, AWWA, WPCF, Washington, D.C.

ASTM (1991) *Standard test method measurement of hydraulic conductivity of saturated porous materials using a flexible wall permeameter*. ASTM D5084-90, Annual Book of ASTM Standards, American Society for Testing and Materials, Philadelphia, Vol. 04.08, pp. 62–69.

Barron, P.F. and Frost, R.L. (1985) Solid-state ^{29}Si NMR examination of the 2:1 ribbon maganesium silicates, sepiolite and palygorskite. *American Mineralogist*, **70**, 758–766.

Bergaya, F. and Vayer, M. (1997) CEC of clays: measurement by adsorption of a copper ethylendiamine complex. *Applied Clay Science*, **12**, 275–280.

Bergaya, F., Theng, B.K.G., and Lagaly, G., editors (2006) *Handbook of Clay Science*. Developments in Clay Science Vol. 1. Elsevier, Amsterdam, pp. 275–278.

Budd, S.M. (1961) The mechanism of chemical reaction between silicate glass and attacking agents. *Physics and Chemistry of Glasses*, **2**, 111–119.

Cai, Y. and Xue, J. (2004) Dissolution behavior and dissolution mechanism of palygorskite in HCl solution. *Progress in Natural Science*, **14**, 2, 47–52.

Carolina, B., Miguel, A.B.M., and Miguel, A.V. (2002) Chemical activation of a kaolinite under acid and alkaline conditions. *Chemistry of Materials*, **14**, 2033–2043.

Chaturvedi, A.K., Pathak, K.C., and Singh, V.N. (1988) Fluoride removal from water by adsorption on china clay. *Applied Clay Science*, **3**, 337–346.

Cody, R.D. and Thompson, G. L. (1976) Quantitative X-ray powder diffraction analysis of clays using an orienting internal standard and pressed disks of bulk shale samples. *Clays and Clay Minerals*, **24**, 224–231.

Dirken, P.J., Jansen, J.B.H., and Schuiling, R.D. (1992) Influence of octahedral polymerization on ^{23}Na and ^{27}Al MAS-NMR in alkali fluoroaluminates. *American Mineralogist*, **77**, 718–724.

Engelhardt, D. and Michel, D. (1987) *High Resolution Solid-state NMR of Silicates and Zeolites.* Wiley, Chichester, UK.

https://doi.org/10.1346/CCMN.2008.0560209 Published online by Cambridge University Press

Fiske, P.S., Nellis, W.J., Xu, Z., and Stebbins, J.F. (1998) Shocked quartz: A ^{29}Si magic-angle-spinning nuclear magnetic resonance study. *American Mineralogist*, **83**, 1285–1292.

Fyfe, C.A., Thomas, J.M., Klinowski, J., and Gobbi, G.C. (1983) Magic-angle-spinning NMR (MAS-NMR) spectroscopy and the structure of zeolites. *Angewandte Chemie*, **22**, 259–336 (English edition).

Gonzalez, F., Pesquera, C., Blanco, C., Benito, I., Mendioroz, S., and Pajares, J.A. (1989) Structural and textural evolution of Al- and Mg-rich palygorskites, I. Under acid treatment. *Applied Clay Science*, **4**, 373–388.

Guggenheim, S. and Koster van Groos, A.F. (2001) Baseline studies of the Clay Minerals Society source clays: Thermal analysis. *Clays and Clay Minerals*, **49**, 433–443.

Hamdi, N., Della, M., and Srasra, E. (2005) Experimental study of the permeability of clays from the potential sites for acid effluent storage. *Desalination*, **185**, 1947–1958.

Imre, D., Laszlo, T., Antonio, F., and Janos, B.N. (1999) The structure of acid treated sepiolites: small-angle X-ray scattering and multi MAS-NMR investigations. *Applied Clay Science*, **14**, 141–160.

Jerry, C.C.C., and Hellmut, E. (2001) High-resolution ^{27}Al ^{19}F solid-state double resonance NMR studies of AlF_3-BaF_2-CaF_2 glasses. *Journal of Non-Crystalline Solids*, **248**, 16–21.

Jozja, N. (2003) Étude de matériaux argileux albanais. Caractérisation «Multi-echelle» d'une bentonite magnésienne. Impact de l'interaction avec le nitrate de plomb sur la perméabilité. PhD thesis, Université d'Orléans, France, 55 pp.

Kau, P.M.H., Smith, D.W., and Binning, P.J. (1997a) The dissolution of kaolin by acidic fluoride wastes. *Soil Science*, **162**, 896–911.

Kau, P.M.H., Smith, D.W., and Binning, P.J. (1997b) Fluoride retention by kaolin. *Journal of Contaminant Hydrology*, **28**, 267–288.

Kau, P.M.H., Smith, D.W., and Binning, P.J. (1998) Experimental sorption of fluoride by kaolinite and bentonite. *Geoderma*, **84**, 89–108.

Kinsey, R.A., Kirkpatrick, R.J., Hower, J., Smith, K.A., and Oldfield, E. (1985) High resolution aluminum-27 and silicon-29 nuclear magnetic resonance studies of layer silicates, including clay minerals. *American Mineralogist*, **70**, 537–548.

Kiyoshi, O., Naoki, A., Yoshikazu, K., Akira, N., and Kenneth, J.D.M. (2006) Solid acidity of 2:1 type clay minerals activated by selective leaching. *Applied Clay Science*, **31**, 185–193.

Komarneni, S., Fyfe, C.A., and Kennedy, G.J. (1986) Detection of non-equivalent Si sites in sepiolite and palygorskite by solid-state ^{29}Si magic angle spinning-nuclear magnetic resonance. *Clays and Clay Minerals*, **34**, 99–102.

Kuang, W., Facey, A.G., and Detellier, C. (2004) Dehydratation and rehydratation of palygorskite and the influence of water on the nanopores. *Clays and Clay Minerals*, **52**, 635–642.

Mackenzie, R.C. (1970) *Differential Thermal Analysis, vol 1. Fundamental Aspects*. Academic Press, London and New York, pp. 478–479.

Madejová, J. and Komadel, P. (2001) Baseline studies of the Clay Minerals Society source clays: Infrared methods. *Clays and Clay Minerals*, **49**, 410–432.

Myriam, M., Suarez, M., and Martin Pozas, J.M. (1998) Structure and textural modifications of palygorskite and sepiolite under acid treatment. *Clays and Clay Minerals*, **46**, 225–236.

Monteiro, S.N., Vieira, C.M.F., and De Carvalho, E.A. (2005) Technological behavior of red ceramics incorporated with brick waste. *Revista Matéria*, **10**, 537–542.

Muller, D., Gessner, W., Behrends, H.J., and Scheler, G. (1981) Determination of the aluminum coordination in aluminum-oxygen compounds by solid-state high resolution ^{27}A1 NMR: *Chemical Physics Letters*, **79**, 59–62.

Peterson, S.R. and Gee, G.W. (1985) Interaction between acidic solutions and clay liners: permeability and neutralisation. *Hydraulic Barriers in Soil and Rock.* ASTM Special Technical Publication, **874**, 229 pp., American Society for Testing and Materials.

Sing, K.S.W., Everett, D.H., Haul, R.A.W., Moscou, L., Pierotti, R.A., Rouquerol, J., and Siemieniewska, T. (1985) Reporting physisorption data for gas/solid systems. *Pure and Applied Chemistry*, **57**, 603–619.

Spearing, D.R. and Stebbins, J.F. (1989) The ^{29}Si NMR shielding tensor in low quartz. *American Mineralogist*, **74**, 956–959.

Suárez, M. and García-Romero, E. (2006) FTIR spectroscopic study of palygorskite: Influence of the composition of the octahedral sheet. *Applied Clay Science*, **31**, 154–163.

Temuujin, J., Jadambaa, Ts., Burmaa, G., Erdenechimeg, Sh., Amarsanaa, J., and MacKenzie, K.J.D. (2004) Characterisation of acid activated montmorillonite clay from Tuulant (Mongolia). *Ceramics International*, **30**, 251–255.

Vanderborgh, N.E. (1968) Evaluation of the lanthanum fluoride membrane electrode response in acidic solution. *Talanta*, **15**, 1009.

Viseras, C. and Lopez-Galindo, A. (1999) Pharmaceutical applications of some Spanish clays – sepiolite, palygorskite, bentonite: some preformulation studies. *Applied Clay Science*, **14**, 69–82.

WHO (World Health Organization) (1993) *Guidelines for Drinking Water Quality*, World Health Organization, Geneva.

(*Received 11 September 2006; revised 10 January 2008; Ms. 1215; A.E. J. Amonette*)